Model Predictive Current Control of Six-Phase Induction Motor Drives Using Virtual Vectors and Space Vector Modulation

Osvaldo Gonzalez, Magno Ayala, Carlos Romero, Larizza Delorme, *Student Member, IEEE*, Jorge Rodas, *Senior Member, IEEE*, Raúl Gregor, Ignacio Gonzalez-Prieto, and Mario J. Durán

***Abstract*—The use of multiphase machines has become a suitable choice in high-performance industry applications through advantages such as lesser torque ripple, enhanced current distribution per phase, and fault-tolerance capability. Among different control approaches for the regulation of multiphase drives, model-based predictive current control (MPCC) is one of the most analyzed strategies due to its adaptability and good dynamic response. However, this approach presents some disadvantages, e.g., high $x-y$ currents and increased harmonic content in the fundamental $\alpha-\beta$ stator currents. Modulation strategies have been combined with MPCC to overcome these shortcomings. This article proposes a modulated MPCC with virtual vectors and space vector modulation for the regulation of an asymmetrical six-phase induction machine to minimize the $x-y$ currents, reduce the harmonic content, and perform improved stator currents tracking compared with other MPCC versions. Experimental tests are provided to demonstrate the quality of the proposed current control strategy.**

***Index Terms*—Modulation strategies, multiphase induction machine, predictive current control, space vector modulation, virtual vectors.**

I. Introduction

RECENTLY, the use of electrical machines with a number of phases greater than three ($n > 3$), known as multiphase machines, has emerged in the literature due to their outstanding characteristics such as better phase current redistribution and enhanced torque production. Multiphase machines can operate in the presence of faults in contrast to their three-phase counterparts [1]. Additionally, multiphase machines are being adopted for high-demanding electric drive applications, for instance, electric ship propulsion, electric vehicles, and renewable energy systems [2]. However, multiphase drives require the development of elaborated control strategies to regulate the system variables (e.g. speed, currents, flux). According to control strategies such as direct torque control (DTC), which is based on hysteresis controllers [3] and the field-oriented control (FOC) with multiple inner proportional-integer (PI) current controllers [4], they have been analyzed over the years to produce a decoupled control of the torque and flux.

Furthermore, nonlinear controllers have been recently implemented to improve the control of multiphase machines [5]–[8]. Model-based predictive control with finite-control-set (FCS-MPC) combined with FOC or DTC scheme is one of the most analyzed strategies for its inherent fast dynamic response as well as the capacity to include various control objectives in comparison to linear controllers, addressed in [9]–[13]. Furthermore, the combination of the sliding-mode controller with FOC has also been studied in the literature to provide a more robust controller [14], [15]. However, the FCS-model-based predictive current control (FCS-MPCC), named MPCC henceforth in the document for simplicity, faces some disadvantages when applied to multiphase machines. Some of them are the large $x-y$ currents which are related to copper losses and large current harmonic content due to the absence of a modulator, resulting in a variable switching frequency [12], [16]. Recent work has been presented to deal with these drawbacks.

In [17], a comparative study of MPCC variants was presented to mitigate the $x-y$ currents for an asymmetrical six-phase induction machine (IM), but the $\alpha-\beta$ currents tracking got worse. Then, an MPCC at a fixed switching frequency (MPCC-FSF) using a switching pattern applied to a two-level six-phase voltage source inverter (2L-6PVSI) was presented in [18], improving the $\alpha-\beta$ currents tracking greatly and the $x-y$ currents reduction, but the improvement is only very effective at a lower mechanical speed of the motor. On the other hand, a new MPCC variant with the name of virtual vectors (VVs) was proposed in [19], which produces an average zero $x-y$ voltages, which reduce the $x-y$ currents dramatically, but at the cost of lowering the

Manuscript received June 10, 2021; revised August 13, 2021 and November 29, 2021; accepted January 1, 2022. Date of publication January 7, 2022; date of current version March 24, 2022. This work was supported by CONACYT-Paraguay under Grant POSG16-05. Recommended for publication by Associate Editor B. Mirafzal. *(Corresponding author: Osvaldo Gonzalez.)*

Osvaldo Gonzalez, Magno Ayala, Carlos Romero, Jorge Rodas, and Raúl Gregor are with the Facultad de Ingenieria, Laboratory of Power and Control Systems, Universidad Nacional de Asuncion, Luque 2060, Paraguay (e-mail: ogonzalez@ing.una.py; mayala@ing.una.py; cromero@ing.una.py; jrodas@ing.una.py; rgregor@ing.una.py).

Larizza Delorme is with the Facultad Politecnica, Universidad Nacional de Asuncion, Luque 2060, Paraguay (e-mail: laridelorme@gmail.com).

Ignacio Gonzalez-Prieto and Mario J. Durán are with the Department of Electrical Engineering, Universidad de Malaga, 29016 Malaga, Spain (e-mail: ignaciogp87@gmail.com; mjduran@uma.es).

Color versions of one or more figures in this article are available at https://doi.org/10.1109/TPEL.2022.3141405.

Digital Object Identifier 10.1109/TPEL.2022.3141405

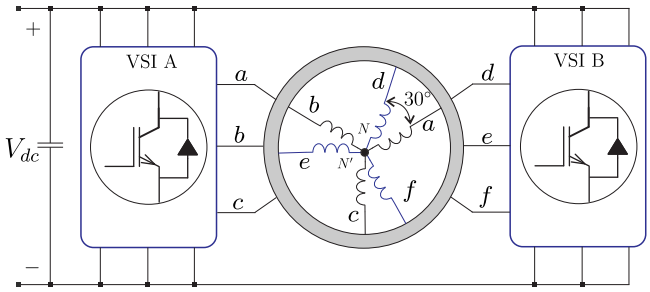

Fig. 1. Six-phase IM fed by 2L-6PVSI.

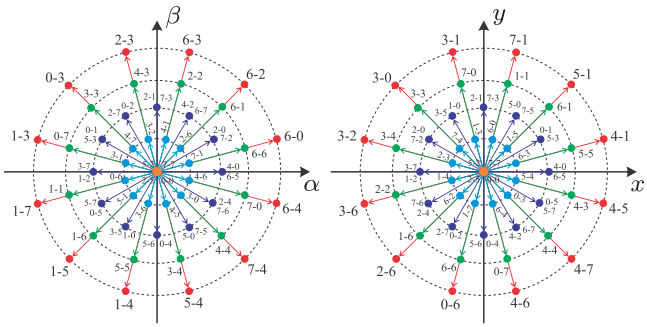

Fig. 2. Voltage vectors for the asymmetrical six-phase IM in the $\alpha - \beta$ and $x - y$ planes.

voltage range in the $\alpha - \beta$ plane. Later, an improvement of the MPCC with VV was presented in [20], where a modulation stage regarding two adjacent VV (4 vectors) is implemented. However, the modulation is restricted to voltage vectors in line with the fixed VV, sparing the control effort of the MPCC. Lastly, a novel modulated MPCC was proposed in [21] to deal with $x - y$ currents and to improve the steady-state quality of stator currents. The improvement was noticed in the steady-state performance and the stability of the whole system, but the improvement of $x - y$ currents reduction was little. In [22], it was shown a direct relationship between the stability of modulated MPCC and the values of sampling frequency and rotor speed for multiphase machines. For this reason, another work regarding a comparative assessment of MPCC with modulation strategies was presented, with simulation results, in [23], where the $x - y$ currents reduction was improved over techniques mentioned above. However, the experimental validation of this article is still missing.

The main contribution of this article is the implementation of a new scheme of the modulated predictive current control strategy using VVs and space vector modulation (SVM). The latter extends the control effort by encompassing the entire area between two virtual space vectors giving more versatility to the control effort by performing a better $\alpha - \beta$ current tracking and reduced $x - y$ currents applied to a six-phase IM fed by 2L-6PVSI. To demonstrate the effectiveness of the proposed strategy compared to the other state-of-the-art MPCC analyzed in this work, experimental tests are presented in terms of mean square error (MSE) and total harmonic distortion (THD) of stator currents under different system conditions.

The rest of this article is organized as follows. The asymmetrical six-phase IM modeling with 2L-6PVSI supply is analyzed in Section II. The fundamental principles of the classic MPCC, its implementation, and their known variants are shown in Section III. Section IV describes the proposed MPCC. The experimental tests for the classic MPCC, MPCC with VV, MPCC-FSF, and the proposed MPCC are addressed and discussed in Section V. Finally, Section VI concludes this article.

II. Six-Phase IM and 2L-6PVSI Mathematical Model

Before applying the proposed strategy, the mathematical model of the system must be taken into account, which is composed of distributed windings for the asymmetrical six-phase IM fed through a 2L-6PVSI connected to a dc-link voltage source (V_{dc}) as shown in Fig. 1. In that context, the two isolated gate bipolar transistors (IGBT) of the power converter per phase can be defined as S_p, with $S_p = 1$ if the upper IGBT is up and the bottom is down or $S_p = 0$ if the contrary occurs. As a result, the switching states of the 2L-6PVSI per phase can be grouped in a vector ($[S_p] = [S_a, S_d, S_b, S_e, S_c, S_f]$), generating 64 possible switching states according to the number of phases of the machine. Thus, using V_{dc} and the S_p vector, the stator phase voltages are calculated as follows:

$$\begin{bmatrix} v_{as} \\ v_{ds} \\ v_{bs} \\ v_{es} \\ v_{cs} \\ v_{fs} \end{bmatrix} = \frac{V_{dc}}{3} \begin{bmatrix} 2 & 0 & -1 & 0 & -1 & 0 \\ 0 & 2 & 0 & -1 & 0 & -1 \\ -1 & 0 & 2 & 0 & -1 & 0 \\ 0 & -1 & 0 & 2 & 0 & -1 \\ -1 & 0 & -1 & 0 & 2 & 0 \\ 0 & -1 & 0 & -1 & 0 & 2 \end{bmatrix} {S_p}^T \tag{1}$$

where T is the transposed operation. Subsequently, to simplify the system modeling, vector space decomposition (VSD) theory based on an invariant amplitude was employed [24]. Thus, stator phase voltages that initially were expressed in phase variables, as specified in (1), are projected into three two-dimensional orthogonal planes, denoted as $\alpha - \beta, x - y$, and $z_1 - z_2$ according to (2). This transformation ensures that the produced planes are entirely decoupled from each other, where the electromechanical energy conversion (flux and torque production) is associated with $\alpha - \beta$ plane, while the system losses are projected in $x - y$ plane, and the $z_1 - z_2$ components are neglected due to the isolated neutral points design of the six-phase IM.

$$T_C = \frac{1}{3} \begin{bmatrix} 1 & \frac{\sqrt{3}}{2} & -\frac{1}{2} & -\frac{\sqrt{3}}{2} & -\frac{1}{2} & 0 \\ 0 & \frac{1}{2} & \frac{\sqrt{3}}{2} & \frac{1}{2} & -\frac{\sqrt{3}}{2} & -1 \\ 1 & -\frac{\sqrt{3}}{2} & -\frac{1}{2} & \frac{\sqrt{3}}{2} & -\frac{1}{2} & 0 \\ 0 & \frac{1}{2} & -\frac{\sqrt{3}}{2} & \frac{1}{2} & \frac{\sqrt{3}}{2} & -1 \\ 1 & 0 & 1 & 0 & 1 & 0 \\ 0 & 1 & 0 & 1 & 0 & 1 \end{bmatrix}. \tag{2}$$

Hence, the voltage vectors, which include 15 redundant and 49 nonredundant vectors obtained from the combination of the switching states, are represented in Fig. 2. Besides, using the state-space representation, the six-phase IM can be written as

$$\dot{X}_{(t)} = A_{(t)}\, X_{(t)} + B_{(t)}\, U_{(t)} + H n_{p(t)} \tag{3}$$

defining $X_{(t)}$ as the state vector, formed by stator and rotor currents as shown in (4), $U_{(t)}$ as the input vector constituted by the stator voltages represented by (5), $n_{p(t)}$ as the process noise, and H as the noise weight matrix. At the same time, $A_{(t)}$ and $B_{(t)}$ are the matrices that contain the electrical parameters of the six-phase IM expressed in (6) and (7), respectively.

$$\begin{aligned} X_{(t)} &= [x_1, x_2, x_3, x_4, x_5, x_6]^T \\ &= [i_{\alpha s}, i_{\beta s}, i_{xs}, i_{ys}, i_{\alpha r}, i_{\beta r}]^T] \end{aligned} \tag{4}$$

$$U_{(t)} = [u_1, u_2, u_3, u_4]^T = [u_{\alpha s}, u_{\beta s}, u_{xs}, u_{ys}]^T \tag{5}$$

$$A_{(t)} = \begin{bmatrix} a_{11} & a_{12} & 0 & 0 & a_{15} & a_{16} \\ a_{21} & a_{22} & 0 & 0 & a_{25} & a_{26} \\ 0 & 0 & a_{33} & 0 & 0 & 0 \\ 0 & 0 & 0 & a_{44} & 0 & 0 \\ a_{51} & a_{52} & 0 & 0 & a_{55} & a_{56} \\ a_{61} & a_{62} & 0 & 0 & a_{65} & a_{66} \end{bmatrix} \tag{6}$$

$$B_{(t)} = \begin{bmatrix} b_{11} & 0 & 0 & 0 \\ 0 & b_{22} & 0 & 0 \\ 0 & 0 & b_{33} & 0 \\ 0 & 0 & 0 & b_{44} \\ b_{51} & 0 & 0 & 0 \\ 0 & b_{62} & 0 & 0 \end{bmatrix} \tag{7}$$

taking into account that

$$a_{11} = a_{22} = -\frac{R_s L_r}{L_s L_r - L_m^2} \qquad a_{12} = -a_{21} = \frac{L_m^2 \omega_r}{L_s L_r - L_m^2}$$

$$a_{15} = a_{26} = \frac{R_r L_m}{L_s L_r - L_m^2} \qquad a_{16} = -a_{25} = \frac{L_m L_r \omega_r}{L_s L_r - L_m^2}$$

$$a_{33} = a_{44} = -\frac{R_s}{L_{ls}} \qquad a_{51} = a_{62} = \frac{R_s L_m}{L_s L_r - L_m^2}$$

$$a_{52} = -a_{61} = -\frac{L_s L_m \omega_r}{L_s L_r - L_m^2} \qquad a_{55} = a_{66} = -\frac{R_r L_s}{L_s L_r - L_m^2}$$

$$a_{56} = -a_{65} = -\frac{L_r L_s \omega_r}{L_s L_r - L_m^2} \qquad b_{11} = b_{22} = \frac{L_r}{L_s L_r - L_m^2}$$

$$b_{33} = b_{44} = \frac{1}{L_{ls}} \qquad b_{51} = b_{62} = -\frac{L_m}{L_s L_r - L_m^2}.$$

Consequently, the six-phase IM equations presented in (3) are written as

$$\begin{aligned} \dot{x_1} &= a_{11}x_1 + a_{12}x_2 + a_{15}x_5 + a_{16}x_6 + b_{11}u_1 \\ \dot{x_2} &= a_{21}x_1 + a_{22}x_2 + a_{25}x_5 + a_{26}x_6 + b_{22}u_2 \\ \dot{x_3} &= a_{33}x_3 + b_{33}u_3 \\ \dot{x_4} &= a_{44}x_4 + b_{44}u_4 \\ \dot{x_5} &= a_{51}x_1 + a_{52}x_2 + a_{55}x_5 + a_{56}x_6 + b_{51}u_1 \\ \dot{x_6} &= a_{61}x_1 + a_{62}x_2 + a_{65}x_5 + a_{66}x_6 + b_{62}u_2 \end{aligned} \tag{8}$$

where $L_s = L_{ls} + L_m$, $L_r = L_{lr} + L_m$, R_s, and R_r are the electrical parameters of the six-phase IM. Then, the input ($U_{(t)}$) and the output ($Y_{(t)}$) vectors, considering the measurement noise ($n_{m(t)}$) in the output, are computed as follows:

$$U_{(t)} = T_C \begin{bmatrix} v_{as} \\ v_{ds} \\ v_{bs} \\ v_{es} \\ v_{cs} \\ v_{fs} \end{bmatrix} \tag{9}$$

$$Y_{(t)} = \begin{bmatrix} 1\,0\,0\,0\,0\,0 \\ 0\,1\,0\,0\,0\,0 \\ 0\,0\,1\,0\,0\,0 \\ 0\,0\,0\,1\,0\,0 \end{bmatrix} X_{(t)} + n_{m(t)}. \tag{10}$$

The torque ($\mathbf{T_e}$) of the six-phase IM and the load torque ($\mathbf{T_L}$) are calculated through the next equations

$$\mathbf{T_e} = 3P\left(\psi_{\alpha s} i_{\beta s} - \psi_{\beta s} i_{\alpha s}\right) \tag{11}$$

$$J_i \dot{\omega}_m + B_i \omega_m = (\mathbf{T_e} - \mathbf{T_L}) \tag{12}$$

$$\omega_m = \frac{\omega_r}{P} \tag{13}$$

J_i, B_i, ω_m, ω_r, $\psi_{\alpha s}$, $\psi_{\beta s}$, and P being the inertia coefficient, the friction coefficient, the rotor mechanical speed, the rotor electrical speed, the stator fluxes, and the number of pole pairs, respectively.

III. MPCC Description

To apply the classic MPCC, a discretization method, obtained from the forward-Euler equation, is applied to (3) to predict the future step of the output variables considering the measurable variables such as the rotor mechanical speed and the stator phase currents. Therefore, the prediction is computed as follows:

$$\hat{X}_{(k+1|k)} = X_{(k)} + f\left(X_{(k)},\, U_{(k)},\, \boldsymbol{\omega}_{r(k)},\, T_s\right) \tag{14}$$

where k and T_s represent the actual sample and the sampling period, respectively.

However, according to (14), rotor currents are nonmeasurable variables. Thus, to face this difficulty, a reduced-order observer needs to be implemented to estimate only the unmeasured variables of $X_{(t)}$. This subject has been addressed in [25]–[27]. In this article, a reduced-order observer based on the Kalman filter (KF) has been implemented because it considers the uncorrelated process and the measurement noises to optimize the filter parameters, thus enhancing the predictions in the controller. Therefore, the discrete state-space modeling can be expressed as

$$\hat{X}_{(k+1|k)} = A_{(k)} X_{(k)} + B_{(k)} U_{(k)} + H n_{p(k)} \tag{15}$$

$$Y_{(k+1|k)} = \begin{bmatrix} 1\,0\,0\,0\,0\,0 \\ 0\,1\,0\,0\,0\,0 \\ 0\,0\,1\,0\,0\,0 \\ 0\,0\,0\,1\,0\,0 \end{bmatrix} X_{(k+1)} + n_{m(k+1)}. \tag{16}$$

The discretized matrices $A_{(k)}$ and $B_{(k)}$ are represented in (17) and (18), respectively. $A_{(k)}$ depends on the present amount of

the rotor electrical speed and it must be updated every sampling period

$$A_{(k)} = \begin{bmatrix} a_{11(k)} & a_{12(k)} & 0 & 0 & a_{15(k)} & a_{16(k)} \\ a_{21(k)} & a_{22(k)} & 0 & 0 & a_{25(k)} & a_{26(k)} \\ 0 & 0 & a_{33(k)} & 0 & 0 & 0 \\ 0 & 0 & 0 & a_{44(k)} & 0 & 0 \\ a_{51(k)} & a_{52(k)} & 0 & 0 & a_{55(k)} & a_{56(k)} \\ a_{61(k)} & a_{62(k)} & 0 & 0 & a_{65(k)} & a_{66(k)} \end{bmatrix} \tag{17}$$

$$B_{(k)} = \begin{bmatrix} b_{11(k)} & 0 & 0 & 0 \\ 0 & b_{22(k)} & 0 & 0 \\ 0 & 0 & b_{33(k)} & 0 \\ 0 & 0 & 0 & b_{44(k)} \\ b_{51(k)} & 0 & 0 & 0 \\ 0 & b_{62(k)} & 0 & 0 \end{bmatrix}. \tag{18}$$

The coefficients of the matrices are detailed in the Appendix.

Besides, another important component in the MPCC to be considered is the cost function (J), which can be expressed according to the variables to be optimized, e.g., harmonic content reduction and switching losses [28]. In this article, the current tracking error in the prediction of the stator currents has been considered. In this regard, the cost function is computed for all control signals, i.e., 64 times for the six-phase IM to obtain the lowest one to be applied in the next sampling period. The current tracking error between the reference ($i^*_{s(k+2)}$) and their predicted values ($\hat{i}_{s(k+2)}$) in the $\alpha-\beta$ and $x-y$ planes is calculated as follows:

$$J = \sqrt{(e_{\alpha s})^2 + (e_{\beta s})^2 + \lambda_{xy}[(e_{xs})^2 + (e_{ys})^2]} \tag{19}$$

where

$$\begin{aligned} e_{\alpha s} &= i^*_{\alpha s(k+2)} - \hat{i}_{\alpha s(k+2)} \\ e_{\beta s} &= i^*_{\beta s(k+2)} - \hat{i}_{\beta s(k+2)} \\ e_{xs} &= i^*_{xs(k+2)} - \hat{i}_{xs(k+2)} \\ e_{ys} &= i^*_{ys(k+2)} - \hat{i}_{ys(k+2)} \end{aligned} \tag{20}$$

which J is based on a four-dimensional distance formula [18], [21].

It must be noted that a second-step ahead prediction is implemented to consider the delay compensation. This fact is produced by a notable amount of time in the computation of the control signals comparable to the sampling period [29], [30]. The tuning parameter (λ_{xy}) in (19) is usually considered in the control of the multiphase machines to provide greater weight to the $\alpha-\beta$ currents over the $x-y$ currents.

A. MPCC With VV

The strategy of the MPCC with VV consists in the use of two aligned non-null voltage vectors, composed by the large vector (filled red circle) and the medium-large vector (filled green circle), as shown in Fig. 3, which are implemented at every sampling period. The dwell time of the vectors (d_l and d_{ml}) are obtained from a system of equations considering the modules of the analyzed vectors. Thus, the MPCC with VV can

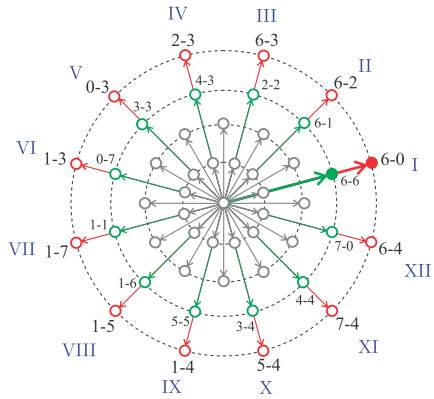

Fig. 3. Space vectors in the $\alpha-\beta$ plane for MPCC with VV.

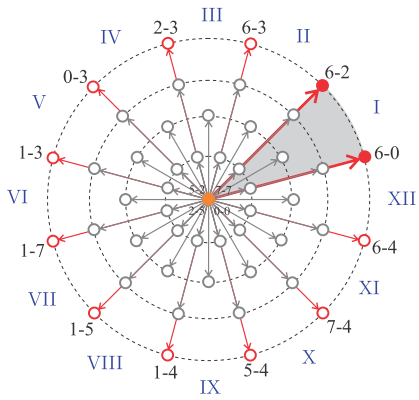

Fig. 4. Space sectors in the $\alpha-\beta$ plane for MPCC-FSF.

be expressed as follows:

$$\mathbf{VV} = d_l V_{\text{large}} + d_{ml} V_{\text{mid-large}} \tag{21}$$

being $d_l = 0.73T_s$ and $d_{ml} = 0.27T_s$, which produces 93% of the actual value of the large vector in $\alpha-\beta$ plane but as well generates zero average value of the $x-y$ currents due to the fact that the two selected vectors have opposite projections in $x-y$ plane [19], [31].

B. MPCC-FSF

The MPCC-FSF establishes each obtainable sector according to the SVM strategy for the 2L-6PVSI in the $\alpha-\beta$ plane [18]. The sectors are formed by two consecutive large vectors or outer vectors (filled red circle) and a null vector (filled orange circle), as depicted in Fig. 4. This strategy calculates the predictions of the two consecutive vectors that minimize the cost function (J) and is performed independently for each vector, whose respective cost functions are named J_0, J_1, and J_2, to find the appropriate sector of the 12 sectors in total and, this procedure is carried out at every sampling period. The predictions are computed according to (19). Also, it can be noted that this procedure only changes in the input vector computation. The MPCC-FSF aims to cover the entire $\alpha-\beta$ plane by using large vectors and these vectors are projected as the smallest ones in the $x-y$ plane providing reduced $x-y$ currents.

Hence, the duty cycles for both the pairs of large vectors and for the null vector are represented by the following equations:

$$d_1 = \frac{\rho}{J_1} \quad d_2 = \frac{\rho}{J_2} \quad d_0 = \frac{\rho}{J_0} \tag{22}$$

$$d_1 + d_2 + d_0 = 1. \tag{23}$$

By solving the above equations, the value of auxiliary variable ρ and the duty cycles, d_1, d_2 and d_0, respectively, can be calculated, which are related to their corresponding cost functions specified as

$$d_1 = \frac{J_0 J_2}{J_0 J_1 + J_1 J_2 + J_0 J_2} \tag{24}$$

$$d_2 = \frac{J_0 J_1}{J_0 J_1 + J_1 J_2 + J_0 J_2} \tag{25}$$

$$d_0 = \frac{J_1 J_2}{J_0 J_1 + J_1 J_2 + J_0 J_2}. \tag{26}$$

This strategy assesses the 12 sectors over a sampling period according to a new cost function defined in (27). The two large vectors which minimize the new cost function are considered to be implemented to the 2L-6PVSI at the next sampling period.

$$J'_{(k+2)} = d_1 J_1 + d_2 J_2. \tag{27}$$

Furthermore, it must be provided with the relationships between the duty cycles and the selected vectors to implement this strategy. The latter can be done by using

$$D_j = \frac{d_0}{2} + d_1 v_{1(j)} + d_2 v_{2(j)} \tag{28}$$

being D_j the duty cycles per phase with $j = (a, d, b, e, c, f)$, where the values of D_j are normalized between 0 and 1 and are compared with a triangular signal to produce a symmetric pulsewidth modulation (PWM) to be applied to the converter.

IV. Proposed MPCC

The proposed MPCC also uses the SVM technique. This modulation strategy allows a vector combination from their respective projections in the $\alpha - \beta$ plane producing the obtainable sectors for the 2L-6PVSI. Subsequently, the proposed MPCC employs five vectors per sector, where each sector is composed of two consecutive large vectors (filled red circle), two consecutive medium-large vectors (filled green circle), and a null vector (filled orange circle). Fig. 5 shows the resulting 12 sectors. The predictions for the vectors and their cost functions are computed in the same way as the previous strategy (19). Hence, the primary purpose of the proposed MPCC is to generate null $x - y$ currents by incorporating the medium-large vectors in the modulation strategy in the stator currents tracking. This fact arises because the medium-large vectors are aligned with the large vectors and they have the same direction in the $\alpha - \beta$ plane; however, large vectors have opposite directions than medium–large vectors in the $x - y$ plane. It is noted that medium–large vectors keep their projections in both planes. Therefore, the proposed MPCC takes advantage of this characteristic to produce the expected results in a similar way to MPCC with VV with the difference that this technique covers the entire area of the voltage space vectors between two VV.

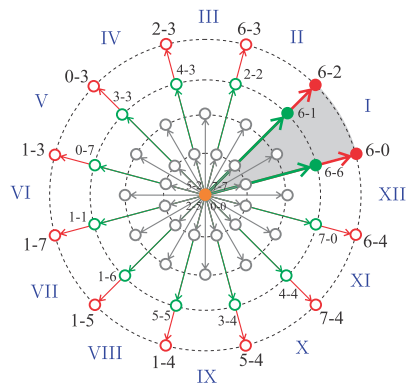

Fig. 5. Space vectors in the $\alpha - \beta$ plane for the proposed MPCC.

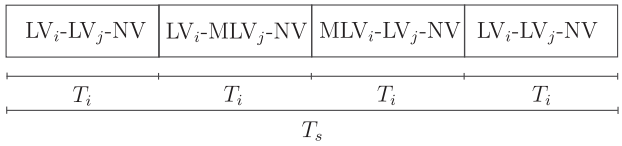

Fig. 6. Applied vector pattern for the proposed MPCC.

In that regard, to implement the proposed MPCC in a digital signal processor (DSP) using the five vectors of each sector and considering the dwell time of the MPCC with VV, a single interrupt routine that is equal to the sampling period has been used. Then, the duty cycles and the cost function are also obtained from (22) to (26) and (27), respectively.

It is worth mentioning that after obtaining the optimal duty cycles for the large vectors, these are also employed for the medium-large vectors to implement the proposed modulation strategy according to the chosen voltage vectors. However, to generate the percentage of time required (which is a function of T_s) for the considered vectors to produce reduced $x - y$ currents and improved $\alpha - \beta$ currents tracking, each large vector must be applied three times (75% of T_s), while each medium-large vector once (25% of T_s). Therefore, to perform the control algorithm once, the interruption routine runs four times, applying the suitable vector combination each time. Note that this approach produces a reduction of four times the original sampling frequency. Moreover, the application of the selected vectors must follow a specific order so they can be synthesized by (28) [18], [21]. For instance, in sector I, the large vectors are applied from V_1 (6-0) to V_2 (6-2) but the combinations between the large vectors and the medium–large vectors are applied in two different ways, first from V_1 (6-0) to V_4 (6-1) and second from V_2 (6-2) to V_3 (6-6), as shown in Fig. 6. The procedure is repeated depending on the location of the current reference. This method enables the synthesis of any voltage vector per sector during the modulation by using (28), which represents the relationship between the duty cycles of every leg of the 2L-6PVSI and the selected vectors. Finally, the duty cycles are compared with a triangular waveform to generate a symmetric PWM to be applied to the VSI. Fig. 7 represents the flowchart of the proposed MPCC.

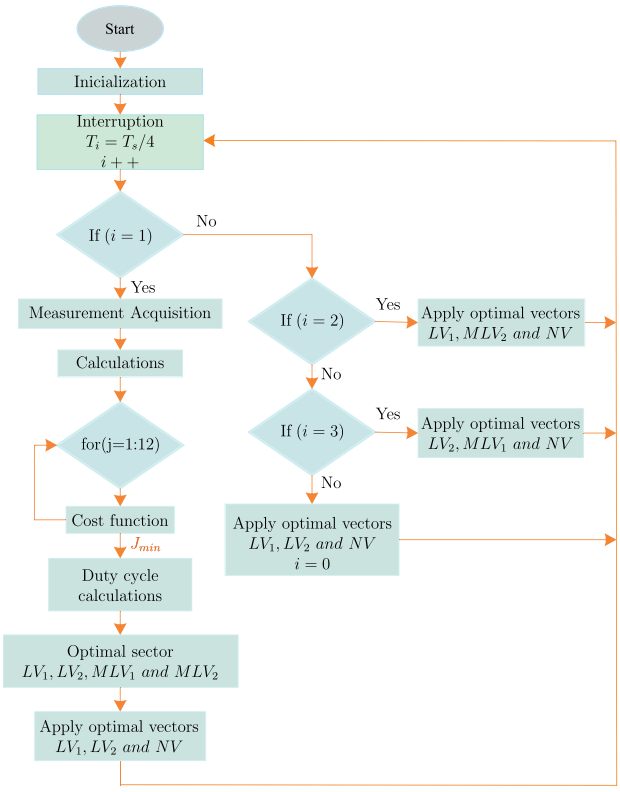

Fig. 7. Flowchart of the proposed MPCC.

Fig. 8. Test bench composed of the 2L-6PVSI, DSP unit control, six-phase IM, and the mechanical load.

TABLE I
ELECTRICAL AND MECHANICAL PARAMETERS OF THE SIX-PHASE IM

Parameter	Value	Parameter	Value
R_r	0.63 Ω	L_s	206.2 mH
R_s	0.62 Ω	P	3
L_{ls}	6.4 mH	P_w	15 kW
L_{lr}	3.5 mH	J_i	0.27 kg.m^2
L_m	66.6 mH	B_i	0.012 kg.m^2/s
L_r	203.3 mH	ω_{r-nom}	1000 r/min

V. EXPERIMENTAL RESULTS

The proposed MPCC technique is tested to analyze its performance compared to classic MPCC, MPCC at FSF, and MPCC with VV through experimental results gathered in the six-phase IM bench.

A. Six-Phase IM Bench Description

The bench is based on a six-phase IM fed by a 2L-6PVSI, using a three-phase diode rectifier from the power grid through a step-down transformer obtaining 325 V for the dc-link. The 2L-6PVSI is controlled by a DSP (TMS320F28335 from Texas Instruments), with an MCK28335 development environment from Technosoft. The results are then processed using MATLAB script. Table I presents the parameters of the six-phase IM determined by stand-still with VSI tests and conventional methods of ac time domain [32], [33].

The current measurements were obtained with current sensors LA 55-P s, with many turns to improve precision at low current amplitude, and it has a frequency bandwidth from dc up to 200 kHz. Those values are then converted to discrete values through a 16-bit A/D converter. The six-phase rotor angle is measured with a 10 000 ppr incremental encoder and the mechanical speed is obtained from it. Finally, a fixed mechanical brake pad, set to approximately 120 N·m, is used as a mechanical load for the six-phase IM. A block diagram of the test bench is shown in Fig. 8 and the employed control scheme of the six-phase IM drive in Fig. 9.

The defined cost function in (19) with $\lambda_{xy} = 0.01$ was selected to evaluate the performance of the proposed MPCC, prioritizing the $\alpha - \beta$ current tracking. The selection of λ_{xy} is made through a heuristic method. However, this value is the same order as the obtained by the optimal procedure proposed in [34]. The process and measurement noise covariances, from (15) and (16), can be estimated by using the autocovariance-least-squared (ALS) method proposed in [27]. The obtained values are $\hat{Q}_w = 0.0022$ and $\hat{R}_v = 0.0022$.

B. Figures of Merit

The performance of the proposed MPCC is analyzed and compared to classic MPCC, MPCC with VV, and MPCC at FSF in steady-state and transient operation. The experimental results show the controllers performance in terms of MSE between the reference and measured stator currents in $\alpha - \beta$ and $x - y$ planes [35]. Finally, THD is calculated in $\alpha - \beta$ plane to

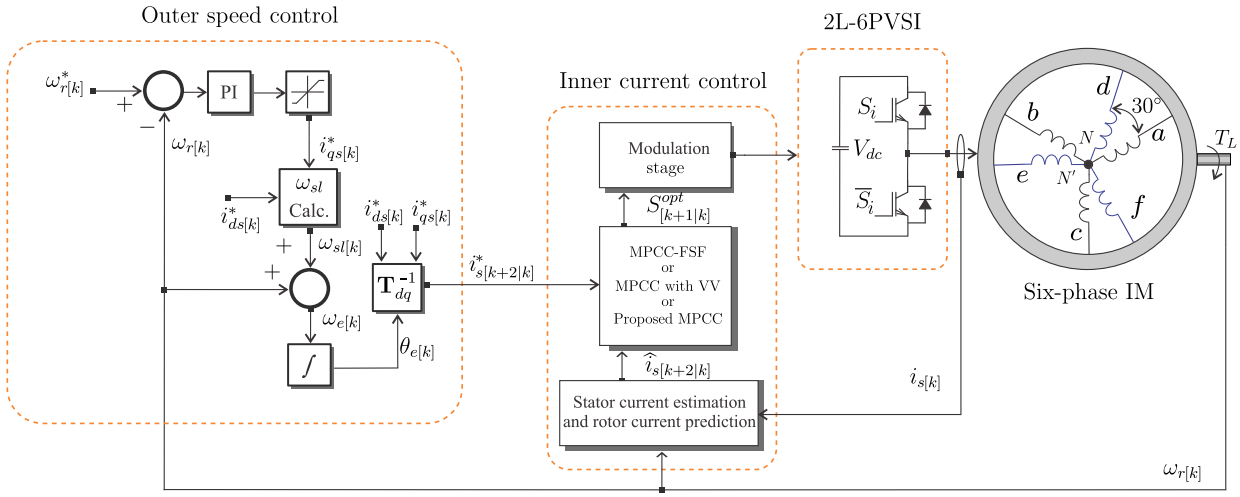

Fig. 9. Control scheme for six-phase IM drive.

TABLE II
AVERAGE SWITCHING FREQUENCY OF THE PROPOSED ALGORITHMS

Algorithm	Sampling Frequency	Average Switching Frequency
Classic MPCC	10 kHz	2.5 kHz
MPCC-FSF	10 kHz	10 kHz
MPCC with VV	5 kHz	4 kHz
Proposed MPCC	5 kHz	20 kHz

complete the study. The MSE is defined as

$$\text{MSE}(i_{s\Phi}) = \sqrt{\frac{1}{N}\sum_{k=1}^{N}(i_{s\Phi}[k] - i^*_{s\Phi}[k])^2} \tag{29}$$

where N is the number of samples, $i^*_{s\Phi}$ the stator currents reference, $i_{s\Phi}$ the measured stator currents, and $\Phi \in \{\alpha,\ \beta,\ x,\ y\}$. At the same time, THD is defined as

$$\text{THD}(i_s) = \sqrt{\frac{1}{i^2_{s1}}\sum_{j=2}^{N}(i_{sj})^2} \tag{30}$$

where i_{s1} is the fundamental component of the stator currents and i_{sj} are the harmonic stator currents.

C. Steady-State Study

For all cases, $x-y$ current references are fixed to zero ($i^*_{xs} = i^*_{ys} = 0$), and d-axis current ($i^*_{ds} = 1.5$ A) has been considered. The sampling frequency in all tests for classic MPCC and MPCC-FSF is 10 kHz, and 5 kHz for MPCC with VV and the proposed MPCC because the sampling frequency is divided by 4 for both techniques and the hardware limit does not allow the further increase. It is worth mentioning that the average switching frequency for all the tested algorithms is shown in Table II. Five steady-state operating points are considered with mechanical rotor speeds of 100–500 r/min.

Table III presents the experimental results for classic MPCC, in terms of MSE of stator currents in $\alpha-\beta$ and $x-y$ planes and THD (%) in $\alpha-\beta$ plane. The results denote good current tracking in $\alpha-\beta$ plane. However, the $x-y$ current reduction is poor, and the performance is similar at higher rotor speed.

TABLE III
STATOR CURRENTS IN $\alpha-\beta$ AND $x-Y$ PLANES, CONSIDERING MSE (A) AND THD (%) FOR CLASSIC MPCC AT DIFFERENT ROTOR SPEEDS

Classic MPCC at f_s = 10 [kHz]					
ω^*_m	MSE_α	MSE_β	MSE_x	MSE_y	THD_α
100	3.25	2.65	14.14	13.04	18.68
200	3.23	2.63	12.85	14.38	19.13
300	3.32	2.89	15.05	14.45	15.56
400	3.33	2.95	14.26	14.22	18.09
500	3.57	3.39	15.12	15.68	17.49

TABLE IV
STATOR CURRENTS IN $\alpha-\beta$ AND $x-Y$ PLANES, CONSIDERING MSE (A) AND THD (%) FOR MPCC-FSF AT DIFFERENT ROTOR SPEEDS

MPCC-FSF at f_s = 10 [kHz]					
ω^*_m	MSE_α	MSE_β	MSE_x	MSE_y	THD_α
100	3.23	2.89	2.19	2.51	13.99
200	4.59	4.42	2.23	2.28	11.85
300	5.01	5.41	2.55	2.76	10.18
400	5.16	5.51	2.46	2.98	10.56
500	5.30	5.23	2.36	2.84	10.09

TABLE V
STATOR CURRENTS IN $\alpha-\beta$ AND $x-Y$ PLANES, CONSIDERING MSE (A) AND THD (%) FOR MPCC WITH VV AT DIFFERENT ROTOR SPEEDS

MPCC with VV at f_s = 5 [kHz]					
ω^*_m	MSE_α	MSE_β	MSE_x	MSE_y	THD_α
100	1.28	1.10	2.68	2.90	9.42
200	1.37	1.25	2.69	2.91	10.86
300	1.51	1.32	2.65	2.95	12.43
400	1.66	1.51	2.66	2.87	14.02
500	1.88	1.75	2.58	2.93	17.07

Table IV presents the results of MPCC-FSF, which shows a far better performance in terms of $x-y$ current reduction compared to classic MPCC. However, the performance is worse for $\alpha-\beta$ current tracking. At the same time, Table V depicts the

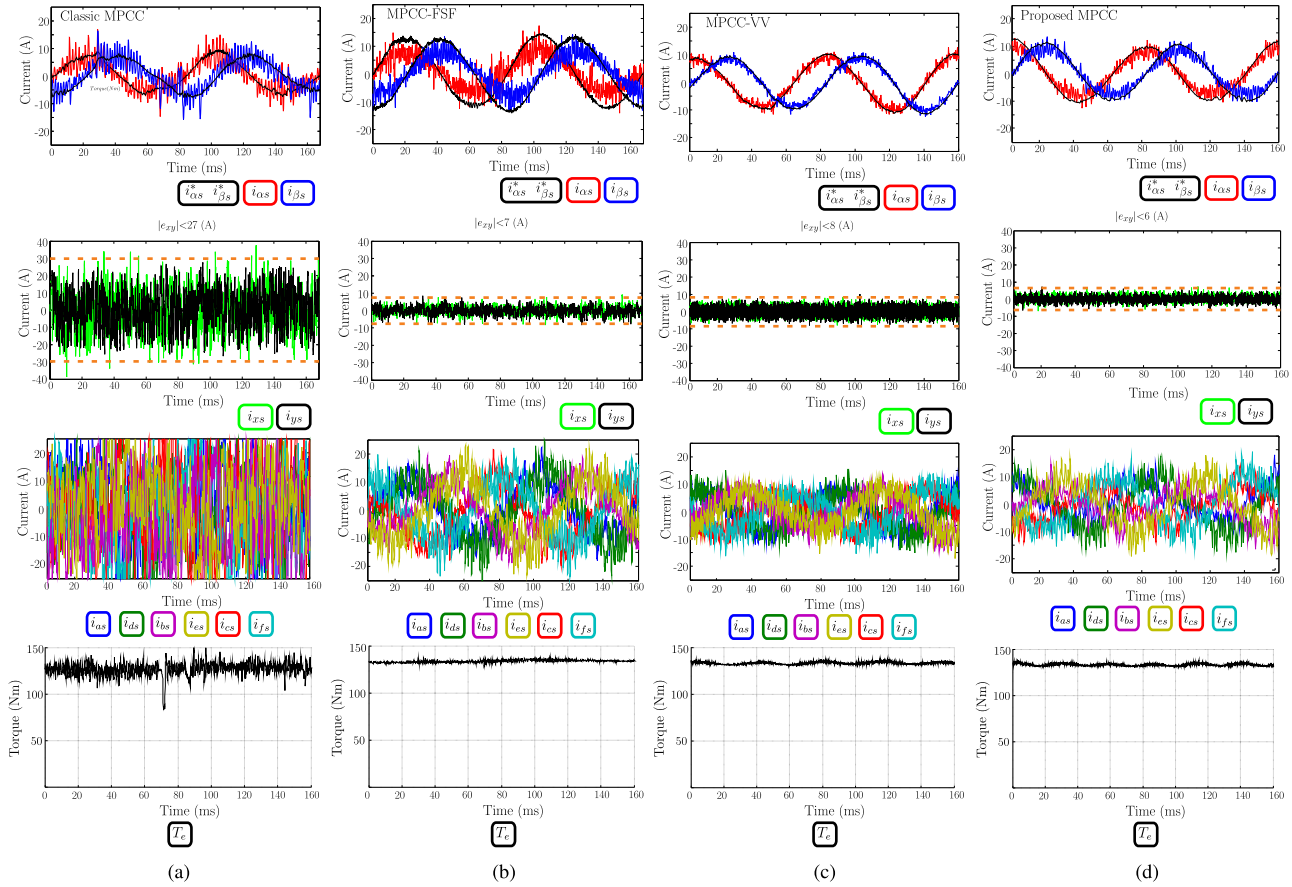

Fig. 10. Performance of stator currents in $\alpha - \beta$ and $x - y$ planes for a rotor speed of 200 (r/min). (a) Classic MPCC. (b) MPCC-FSF. (c) MPCC with VV. (d) Proposed MPCC.

TABLE VI
STATOR CURRENTS IN $\alpha - \beta$ AND $x - Y$ PLANES, CONSIDERING MSE (A) AND THD (%) FOR THE PROPOSED MPCC AT DIFFERENT ROTOR SPEEDS

Proposed MPCC at f_s = 5 [kHz]					
ω_m^*	MSE$_\alpha$	MSE$_\beta$	MSE$_x$	MSE$_y$	THD$_\alpha$
100	2.34	2.07	1.84	1.90	10.11
200	2.48	2.25	1.76	1.74	10.89
300	2.49	2.29	1.95	1.91	12.06
400	2.97	2.76	1.92	1.89	12.04
500	3.01	2.90	2.02	1.91	16.14

performance of MPCC with VV which significantly improves the tracking and reduction of $\alpha - \beta$ and $x - y$ currents compared to classic MPCC. Table VI exposes the proposed MPCC in terms of currents tracking. It can be seen that the proposed MPCC greatly improves the $x - y$ current reduction compared to the other techniques. At the same time, the THD is also better, and the $\alpha - \beta$ currents tracking is good compared with classic MPCC.

Fig. 10 shows the stator current tracking in $\alpha - \beta$ and $x - y$ planes and the electromagnetic torque for classic MPCC, MPCC-FSF. MPCC with VV, and the proposed MPCC. The operations were tested at a rotor speed of 200 r/min for all the techniques. The figures reveal that $x - y$ currents are considerably lower for the proposed MPCC than the other MPCC techniques and proper current tracking in the $\alpha - \beta$ plane.

D. High-Speed Operation

A high-speed operation is performed, so the dc-link is increased to 575 V to operate at nominal magnetic flux. The current ripple is also increased as the voltage switching is higher. The nominal condition results are shown in Fig. 11. The system performance is decreased, but it operates very well with almost nominal torque.

E. Transient Study

For a transient operation, a step modification in the rotor speed is considered from 200 to −200 r/min (reversal condition). Fig. 12 presents a dynamic test (q current tracking), which reveals the transient operation of classic MPCC (a), MPCC with VV (b), MPCC-FSF (c), and the proposed MPCC (d) for a step-change in the q current (i_{qs}^*). The dynamic performance is obtained through a reversal condition of the rotor speed (ω_m^*). The overshoot and reaching time of all the techniques are very similar, as for the proposed MPCC is approximately 12.5% and 0.5 ms, respectively.

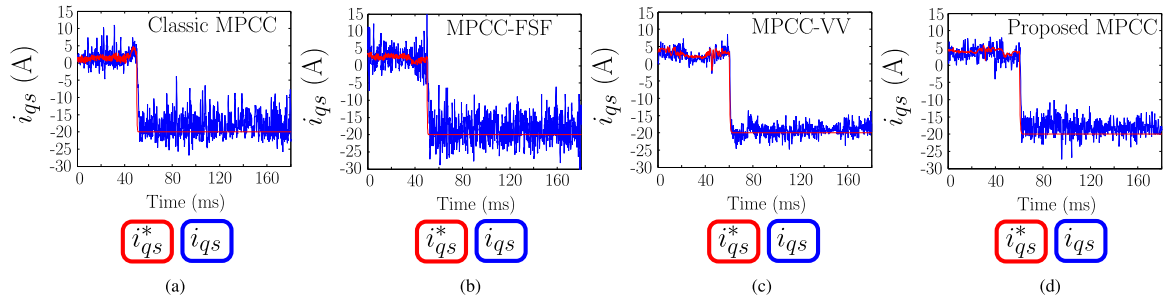

Fig. 11. Transient response in q-axis of stator current for a rotor speed change from 200 r/min to -200 r/min: (a) Classic MPCC. (b) MPCC-FSF. (c) MPCC with VV. (d) Proposed MPCC.

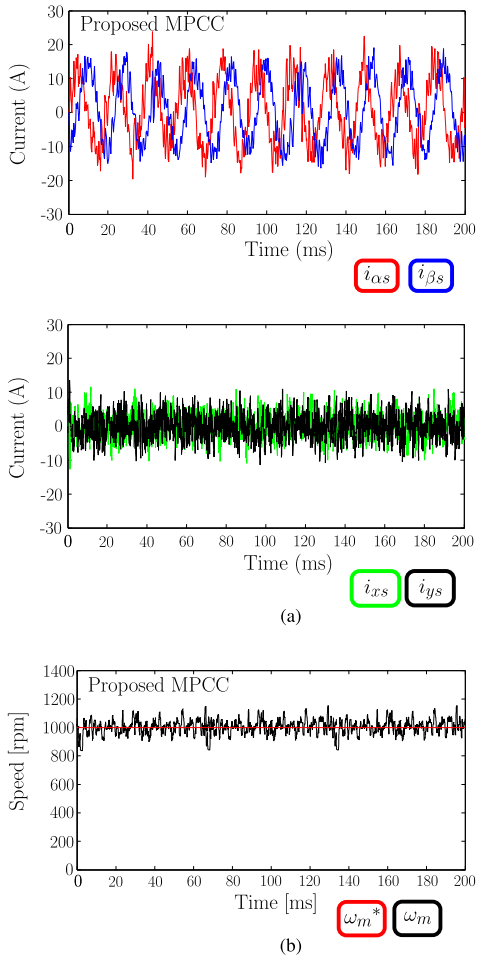

Fig. 12. Performance at nominal condition of: (a) stator currents in $\alpha - \beta$ and $x - y$ planes; (b) rotor mechanical speed.

TABLE VII
ANALYSIS OF STATOR CURRENTS UNDER VARIATION OF L_m

ω_m^* = 400 [rpm]					
Techniques	MSE_α	MSE_β	MSE_x	MSE_y	THD_α
Classic MPCC	3.12	2.93	13.92	14.91	20.83
MPCC with VV	2.12	1.73	2.83	3.08	14.48
MPCC-FSF	4.46	2.70	2.56	2.59	12.82
Proposed MPCC	3.13	2.52	1.79	1.73	10.27

TABLE VIII
COMPARATIVE ANALYSIS (%) OF THE PROPOSED MPCC OVER CLASSIC MPCC, MPCC-FSF, AND MPCC WITH VV

Proposed MPCC over classic MPCC			
ω_m^*	$\text{MSE}_{\alpha\beta}$	MSE_{xy}	THD_α
100	+25.25	+86.23	+45.88
200	+19.28	+87.15	+43.07
300	+23.03	+86.92	+22.49
400	+8.76	+86.62	+33.44
500	+15.09	+87.24	+7.72
Proposed MPCC over MPCC-FSF			
100	+27.94	+20.43	+27.73
200	+47.50	+22.40	+8.10
300	+54.13	+27.31	-18.47
400	+46.30	+29.96	-14.02
500	+43.87	+24.42	-59.96
Proposed MPCC over MPCC with VV			
100	-85.29	+32.98	-7.32
200	-80.53	+37.50	-0.27
300	-68.90	+31.07	+2.98
400	-80.76	+31.10	+14.12
500	-62.81	+28.68	+5.45

F. Robustness Study

The robustness study consists of comparing the controllers at the nominal L_m value and a variation of 25% of the nominal value, as L_m is considered the most sensitive parameter in six-phase IM [10], [36]. This article is performed by considering the effect of magnetic saturation of the six-phase IM, where L_m value typically changes in approximately that ratio. Table VII presents the control performance with an L_m change of 25% of the nominal value to analyze the control robustness parameter sensitivity. The results reveal that the four techniques present considerable robustness as the figures of merit do not change much compared to nominal L_m. Notably, the proposed MPCC presents slightly better results in terms of MSE and the THD is moderately worse, but all values remain in a similar range.

G. Comparative Analysis

Table VIII presents a comparative analysis of the performance all the analyzed MPCC techniques, in terms of %, where positive (+) and negative (−) values mean improvement and deterioration, respectively, which is obtained as follows:

$$\text{Imp}\ (\%) = 100\frac{\text{refMPCC}_{\text{data}} - \text{proposedMPCC}_{\text{data}}}{\text{refMPCC}_{\text{data}}} \quad (31)$$

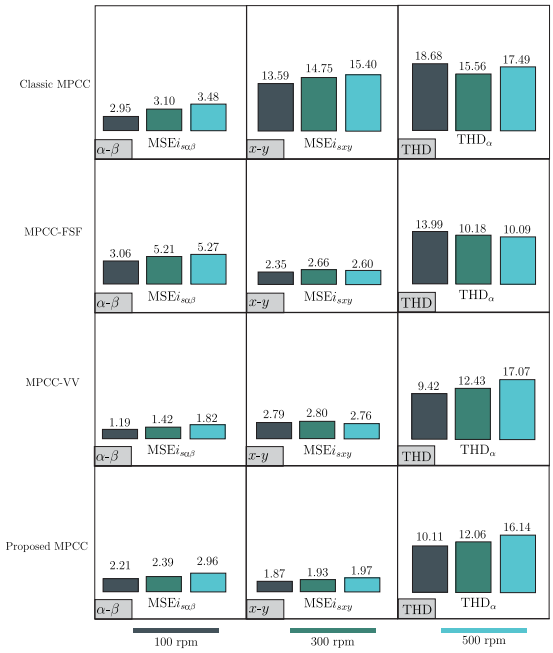

Fig. 13. Performance analysis of stator currents in $\alpha-\beta$ and $x-y$ planes, taking into account MSE (A) and THD (%) for all current controllers at different rotor speeds.

where "data" could be MSE of stator currents in $\alpha-\beta$ and $x-y$ planes or THD of $\alpha-\beta$ stator currents and refMPCC could be classic MPCC, MPCC-FSF, and MPCC with VV. Finally, a performance analysis of stator currents has been included and depicted in Fig. 13 in $\alpha-\beta$ and $x-y$ planes, taking into account the MSE (A) and the THD (%) for all MPCC techniques.

Finally, to measure the computational burden, the number of floating-point operations (FPOs) has been considered as a figure of merit for each MPCC. In that regard, the voltage vectors involved in each predictive control have been considered, representing the number of iterations carried out in every sampling period. In other words, the total number of FPOs in every iteration is related to the prediction computation, the cost function minimization, the second-step prediction process, and the modulation stage. Consequently, the computational burden in terms of FPOs for each MPCC is 3822 FPOs (classic MPCC), 2314 FPOs (MPCC-FSF), 1040 FPOs (MPCC with VV), and 2470 FPOs (proposed MPCC), respectively.

VI. Conclusion

The article proposes implementing a modulation strategy with VVs and SVM applied to an asymmetrical six-phase IM. The strategy has been developed to enhance the stator current tracking in the $\alpha-\beta$ plane and to produce null $x-y$ currents using large, medium-large, and null vectors. Experimental tests are done to prove the effectiveness of the proposed MPCC compared to other strategies such as classic MPCC, MPCC with VV, and the MPCC-FSF under diverse conditions such as different rotor mechanical speeds, steady, and transient operations. The figures of merit of the MPCC with VV and MPCC-FSF show that these controllers are viable alternatives to classic MPCC. Both presents a notable reduction of the $x-y$ currents, noting that MPCC with VV has better $\alpha-\beta$ current tracking than MPCC-FSF. On the other hand, the proposed MPCC, which uses the characteristics of MPCC with VV and MPCC-FSF, has been demonstrated to be the best alternative in terms of $x-y$ currents reduction and THD analysis. But in terms of MSE in the $\alpha-\beta$ plane, the MPCC with VV presents slightly better results than the proposed MPCC followed by the other strategies. In transient conditions, the results of the four controllers showed good dynamic performance. Finally, a robustness test has been implemented where the controllers presented good behavior to the variation of the parameter under study. It is important to mention that the proposed MPCC has been implemented in a large six-phase IM (15 kW), making it suitable for medium power applications.

Appendix

$$a_{11(k)} = a_{22(k)} = 1 - \frac{R_s L_r T_s}{L_s L_r - L_m^2}$$

$$a_{12(k)} = -a_{21(k)} = \frac{L_m^2 \omega_{r(k)} T_s}{L_s L_r - L_m^2}$$

$$a_{15(k)} = a_{26(k)} = \frac{R_r L_m T_s}{L_s L_r - L_m^2}$$

$$a_{16(k)} = -a_{25(k)} = \frac{L_m L_r \omega_{r(k)} T_s}{L_s L_r - L_m^2}$$

$$a_{33(k)} = a_{44(k)} = 1 - \frac{R_s T_s}{L_{ls}}$$

$$a_{51(k)} = a_{62(k)} = \frac{R_s L_m T_s}{L_s L_r - L_m^2}$$

$$a_{52(k)} = -a_{61(k)} = -\frac{L_s L_m \omega_{r(k)} T_s}{L_s L_r - L_m^2}$$

$$a_{55(k)} = a_{66(k)} = 1 - \frac{R_r L_s T_s}{L_s L_r - L_m^2}$$

$$a_{56(k)} = -a_{65(k)} = -\frac{L_r L_s \omega_{r(k)} T_s}{L_s L_r - L_m^2}$$

$$b_{11(k)} = b_{22(k)} = \frac{L_r T_s}{L_s L_r - L_m^2}$$

$$b_{33(k)} = b_{44(k)} = \frac{T_s}{L_{ls}}$$

$$b_{51(k)} = b_{62(k)} = -\frac{L_m T_s}{L_s L_r - L_m^2}.$$

References

[1] M. J. Duran, E. Levi, and F. Barrero, *Multiphase Electric Drives: Introduction*. Hoboken, NJ, USA: Wiley, 2017, pp. 1–26.

[2] R. Bojoi, S. Rubino, A. Tenconi, and S. Vaschetto, "Multiphase electrical machines and drives: A viable solution for energy generation and transportation electrification," in *Proc. Int. Conf. Expo. Elect. Power Eng.*, 2016, pp. 632–639.

[3] E. Levi, R. Bojoi, F. Profumo, H. Toliyat, and S. Williamson, "Multiphase induction motor drives-a technology status review," *IET Electr. Power Appl.*, vol. 1, no. 4, pp. 489–516, 2007.
[4] F. Barrero and M. J. Duran, "Recent advances in the design, modeling, and control of multiphase machines: Part I," *IEEE Trans. Ind. Electron.*, vol. 63, no. 1, pp. 449–458, Jan. 2016.
[5] Y. Kali *et al.*, "Time delay estimation based discrete-time super-twisting current control for a six-phase induction motor," *IEEE Trans. Power Electron.*, vol. 35, no. 11, pp. 12570–12580, Nov. 2020.
[6] A. Gonzalez-Prieto, I. Gonzalez-Prieto, and M. J. Duran, "Smart voltage vectors for model predictive control of six-phase electric drives," *IEEE Trans. Ind. Electron.*, vol. 68, no. 10, pp. 9024–9035, Oct. 2021.
[7] A. Bhowate, M. V. Aware, and S. Sharma, "Predictive torque control of five-phase induction motor drive using successive cost-functions for CMV elimination," *IEEE Trans. Power Electron.*, vol. 36, no. 12, pp. 14133–14141, Dec. 2021.
[8] J. Xu, M. Odavic, Z. Q. Zhu, Z. Wu, and N. Freire, "Modulation restraint analysis of space vector PWM for dual three-phase machines under vector space decomposition," *IEEE Trans. Power Electron.*, vol. 36, no. 12, pp. 14491–14507, Dec. 2021.
[9] F. Barrero, M. R. Arahal, R. Gregor, S. Toral, and M. J. Durán, "A proof of concept study of predictive current control for VSI-driven asymmetrical dual three-phase AC machines," *IEEE Trans. Ind. Electron.*, vol. 56, no. 6, pp. 1937–1954, Jun. 2009.
[10] F. Wang, Z. Zhang, X. Mei, J. Rodríguez, and R. Kennel, "Advanced control strategies of induction machine: Field oriented control, direct torque control and model predictive control," *Energies*, vol. 11, no. 1, pp. 120–132, 2018.
[11] O. Gonzalez, M. Ayala, J. Rodas, R. Gregor, G. Rivas, and J. Doval-Gandoy, "Variable-speed control of a six-phase induction machine using predictive-fixed switching frequency current control techniques," in *Proc. 9th IEEE Int. Symp. Power Electron. Distrib. Gener. Syst.*, 2018, pp. 1–6.
[12] S. Kouro, M. A. Perez, J. Rodriguez, A. M. Llor, and H. A. Young, "Model predictive control: MPC's role in the evolution of power electronics," *IEEE Ind. Electron. Mag.*, vol. 9, no. 4, pp. 8–21, Dec. 2015.
[13] J. Rodas, I. Gonzalez-Prieto, Y. Kali, M. Saad, and J. Doval-Gandoy, "Recent advances in model predictive and sliding mode current control techniques of five-phase and six-phase induction machines," *Front. Energy Res.*, 2021.
[14] Y. Kali *et al.*, "Current control of a six-phase induction machine drive based on discrete-time sliding mode with time delay estimation," *Energies*, vol. 12, no. 1, pp. 170–186, 2019.
[15] Y. Kali, M. Saad, J. Doval-Gandoy, J. Rodas, and K. Benjelloun, "Discrete sliding mode control based on exponential reaching law and time delay estimation for an asymmetrical six-phase induction machine drive," *IET Electr. Power Appl.*, vol. 13, no. 11, pp. 1660–1671, 2019.
[16] P. Gonçalves, S. Cruz, and A. Mendes, "Finite control set model predictive control of six-phase asymmetrical machines–An overview," *Energies*, vol. 12, no. 24, 2019, Art. no. 4693.
[17] M. Ayala, J. Doval-Gandoy, J. Rodas, O. Gonzalez, and R. Gregor, "Current control designed with model based predictive control for six-phase motor drives," *ISA Trans.*, vol. 98, pp. 496–504, 2020.
[18] O. Gonzalez, M. Ayala, J. Doval-Gandoy, J. Rodas, R. Gregor, and M. Rivera, "Predictive-fixed switching current control strategy applied to six-phase induction machine," *Energies*, vol. 12, no. 12, 2019, Art. no. 2294.
[19] I. Gonzalez-Prieto, M. J. Duran, J. J. Aciego, C. Martin, and F. Barrero, "Model predictive control of six-phase induction motor drives using virtual voltage vectors," *IEEE Trans. Ind. Electron.*, vol. 65, no. 1, pp. 27–37, Jan. 2018.
[20] J. J. Aciego, I. Gonzalez-Prieto, M. Duran, M. Bermudez, and P. Salas-Biedma, "Model predictive control based on dynamic voltage vectors for six-phase induction machines," *IEEE J. Emerg. Sel. Topics Power Electron.*, vol. 9, no. 3, pp. 2710–2722, Jun. 2021.
[21] M. Ayala, J. Doval-Gandoy, J. Rodas, O. Gonzalez, R. Gregor, and M. Rivera, "A novel modulated model predictive control applied to six-phase induction motor drives," *IEEE Trans. Ind. Electron.*, vol. 68, no. 5, pp. 3672–3682, May 2021.
[22] M. Ayala, J. Doval-Gandoy, O. Gonzalez, J. Rodas, R. Gregor, and M. Rivera, "Experimental stability study of modulated model predictive current controllers applied to six-phase induction motor drives," *IEEE Trans. Power Electron.*, vol. 36, no. 11, pp. 13275–13284, Nov. 2021.
[23] O. González *et al.*, "Comparative assessment of model predictive current control strategies applied to six-phase induction machines," in *Proc. IEEE Int. Conf. Ind. Technol.*, 2020, pp. 1037–1043.
[24] Y. Zhao and T. Lipo, "Space vector PWM control of dual three-phase induction machine using vector space decomposition," *IEEE Trans. Ind. Electron.*, vol. 31, no. 5, pp. 1100–1109, Sep./Oct. 1995.
[25] J. Rodas, F. Barrero, M. R. Arahal, C. Martin, and R. Gregor, "On-line estimation of rotor variables in predictive current controllers: A case study using five-phase induction machines," *IEEE Trans. Ind. Electron.*, vol. 63, no. 9, pp. 5348–5356, Sep. 2016.
[26] C. Martin, M. R. Arahal, F. Barrero, and M. J. Durán, "Five-phase induction motor rotor current observer for finite control set model predictive control of stator current," *IEEE Trans. Ind. Electron.*, vol. 63, no. 7, pp. 4527–4538, Jul. 2016.
[27] J. Rodas, C. Martin, M. R. Arahal, F. Barrero, and R. Gregor, "Influence of covariance-based ALS methods in the performance of predictive controllers with rotor current estimation," *IEEE Trans. Ind. Electron.*, vol. 64, no. 4, pp. 2602–2607, Apr. 2017.
[28] J. Rodriguez *et al.*, "State of the art of finite control set model predictive control in power electronics," *IEEE Trans Ind. Informat.*, vol. 9, no. 2, pp. 1003–1016, May 2013.
[29] M. Arahal, F. Barrero, S. Toral, M. Duran, and R. Gregor, "Multi-phase current control using finite-state model-predictive control," *Control Eng. Pract.*, vol. 17, no. 5, pp. 579–587, 2009.
[30] J. Rodriguez and P. Cortes, *Predictive Control of Power Converters and Electrical Drives*, vol. 40. Hoboken, NJ, USA: Wiley, 2012.
[31] J. J. Aciego, I. G. Prieto, and M. J. Duran, "Model predictive control of six-phase induction motor drives using two virtual voltage vectors," *IEEE J. Emerg. Sel. Topics Power Electron.*, vol. 7, no. 1, pp. 321–330, Mar. 2019.
[32] A. G. Yepes *et al.*, "Parameter identification of multiphase induction machines with distributed windings—Part 1: Sinusoidal excitation methods," *IEEE Trans. Energy Convers.*, vol. 27, no. 4, pp. 1056–1066, Dec. 2012.
[33] J. A. Riveros *et al.*, "Parameter identification of multiphase induction machines with distributed windings—Part 2: Time-domain techniques," *IEEE Trans. Energy Convers.*, vol. 27, no. 4, pp. 1067–1077, Dec. 2012.
[34] H. Fretes *et al.*, "Pareto optimal weighting factor design of predictive current controller of a six-phase induction machine based on particle swarm optimization algorithm," *IEEE Trans. Emerg. Sel. Topics Power Electron*., to be published, doi: 10.1109/JESTPE.2021.3100687.
[35] G. I. Rivas-Martínez, J. Rodas, and J. D. Gandoy, "Statistical tools to evaluate the performance of current control strategies of power converters and drives," *IEEE Trans. Instrum. Meas.*, vol. 70, Mar. 2021, Art. no. 1006111.
[36] L. Delorme, M. Ayala, J. Rodas, R. Gregor, O. Gonzalez, and J. Doval-Gandoy, "Comparison of the effects on stator currents between continuous model and discrete model of the three-phase induction motor in the presence of electrical parameter variations," in *Proc. IEEE Int. Conf. Ind. Technol*., 2020, pp. 151–156.

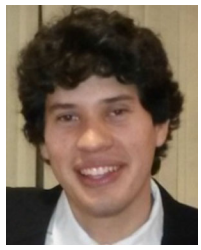

Osvaldo Gonzalez was born in Asunción, Paraguay. He received the B.Eng. degree in electronic engineering from the Universidad Nacional deAsunción (UNA), Luque, Paraguay, in 2014, and the M.Sc. and Ph.D. degrees in power electronics from the Engineering Faculty, UNA, Luque, Paraguay, in 2017 and 2021, respectively.

Since 2015, he has been a Research Assistant with the Laboratory of Power and Control System, UNA. His research interests include the control of multiphase motors.

Magno Ayala received the B.Eng. degree in electronic engineering from the Universidad Nacional de Asunción (UNA), Luque, Paraguay, in 2014, and the M.Sc. and Ph.D. degrees in power electronics from Engineering Faculty, UNA, Luque, Paraguay, in 2017 and 2020, respectively.

Since 2015, he has been a Research Assistant with the Laboratory of Power and Control System, UNA. His research interests include the control of multiphase ac machines.

Dr. Ayala was the recipient of the Highest Award for Researcher at the national level upon being awarded the 2020 National Science Prize in 2020 and an International Award for the Best Scientific Article at an International Conference of the year 2020 from the IEEE Industrial Electronics Society (IES) in 2021.

Carlos Romero received the B.Eng. degree in electronic engineering and the M.Sc. degree in power electronics both from the Universidad Nacional de Asunción (UNA), Luque, Paraguay, in 2014 and 2018, respectively.

Since 2015, he has been a Research Assistant with Engineering Faculty, UNA.

Larizza Delorme (Student Member, IEEE) was born in Asunción, Paraguay in 1990. She received the B.Eng. degree in electronic engineering with emphasis in industrial control from the Universidad Nacional de Asunción (UNA), Luque, Paraguay, in 2017, and the M.Sc. degree in electronic engineering with emphasis on renewable energies and energy efficiency from the Universidad del Cono Sur de las Américas, Asunción, Paraguay, in 2020.

She is currently a Research Assistant with the Laboratory of Power and Control System (LSPyC), UNA. Her research interests include modeling, simulation, and control of multiphase drives.

Jorge Rodas (Senior Member, IEEE) was born in Asunción, Paraguay, in 1984. He received the B.Eng. degree in electronic engineering from the Universidad Nacional de Asunción (UNA), Luque, Paraguay, in 2009, the M.Sc. degrees from the Universidad de Vigo, Vigo, Spain, in 2012, and the Universidad de Sevilla, Sevilla, Spain, in 2013, the joint-university Ph.D. degree from the UNA, Luque, Paraguay, and the Universidad de Sevilla, in 2016, and the master's degree from the National Defense Council, Paraguay, in 2021.

Since 2011, he has been with the Faculty of Engineering, Laboratory of Power and Control Systems (LSPyC), UNA, where he is currently a Professor. In 2017, he made a research stay at the Power Electronics and Industrial Control Research Group, École de Technologie Supérieure, Montreal, Canada. His research interests include applications of advanced control to real-world problems. His current research interests include applying model predictive control and nonlinear control to power electronic converters, renewable energy conversion systems, electric motor drives, and robotic systems (especially drones).

Dr. Rodas was a recipient of the Paraguayan National Science Award in 2020. He was a Guest Editor for *Energies* (MDPI). He is an Associate Editor for *Alexandria Engineering Journal* (Elsevier) and a Guest Editor for the IEEE JOURNAL OF EMERGING AND SELECTED TOPICS IN POWER ELECTRONICS, *World Electric Vehicle Journal (MDPI)*, and *Frontiers in Energy Research*.

Raúl Gregor was born in Asunción, Paraguay, in 1979. He received the bachelor's degree in electronic engineering from the Catholic University of Asunción, Asunción, Paraguay, in 2005, and the M.Sc. and Ph.D. degrees in electronic, signal processing, and communications from the Higher Technical School of Engineering (ETSI), University of Seville, Seville, Spain, in 2008 and 2010, respectively. Since March 2010, he has been the Head of the Engineering Faculty, Laboratory of Power and Control System (LSPyC), National University of Asunción, Asunción, Paraguay. He has authored or coauthored about 40 technical papers in the field of power electronics and control systems, six of which have been published in high-impact factor journals. His research interests include multiphase drives, advanced control of power converters topologies, quality of electrical power, renewable energy, modeling, simulation, optimization and control of power systems, smart metering and smart grids, and predictive control.

Dr. Gregor was a recipient of the Best Paper Award from the IEEE TRANSACTIONS ON INDUSTRIAL ELECTRONICS, Industrial Electronics Society, in 2010, and the Best Paper Award from the *IET Electric Power Applications*, in 2012.

Ignacio Gonzalez-Prieto was born in Malaga, Spain, in 1987. He received the Industrial Engineer and M.Sc. degrees in fluid mechanics from the University of Malaga, Malaga, Spain, in 2012 and 2013, respectively, and the Ph.D. degree in electronic engineering from the University of Seville, Sevilla, Spain, in 2016.

His research interests include multiphase machines, wind energy systems, and electrical vehicles.

Mario J. Durán was born in Bilbao, Spain, in 1975. He received the M.Sc. and Ph.D. degrees in electrical engineering from the University of Malaga, Malaga, Spain, in 1999 and 2003, respectively.

He is currently a Full Professor with the Department of Electrical Engineering, University of Malaga. His research interests include modeling and control of multiphase drives and renewable energies conversion systems.